AGU PUBLICATIONS

Geophysical Research Letters

RESEARCH LETTER

10.1002/2016GL071155

Key Points:
- Methane mole fraction and $\delta^{13}C$ have been measured from samples collected by UASs on Ascension Island over two campaigns
- CH_4 mole fraction increases above the TWI, but isotopes have no consistent signal indicating input from Africa is close to background
- The campaigns illustrate the usefulness of UAS sampling and Ascension's value for atmospheric measurement in an understudied region

Supporting Information:
- Supporting Information S1

Correspondence to:
R. Brownlow,
Rebecca.Brownlow.2009@live.rhul.ac.uk

Citation:
Brownlow, R., et al. (2016), Methane mole fraction and $\delta^{13}C$ above and below the trade wind inversion at Ascension Island in air sampled by aerial robotics, *Geophys. Res. Lett.*, *43*, 11,893–11,902, doi:10.1002/2016GL071155.

Received 13 SEP 2016
Accepted 3 NOV 2016
Accepted article online 5 NOV 2016
Published online 19 NOV 2016

Methane mole fraction and $\delta^{13}C$ above and below the trade wind inversion at Ascension Island in air sampled by aerial robotics

R. Brownlow[1], D. Lowry[1], R. M. Thomas[2,3], R. E. Fisher[1], J. L. France[4], M. Cain[5], T. S. Richardson[6], C. Greatwood[6], J. Freer[7], J. A. Pyle[5], A. R. MacKenzie[2,3], and E. G. Nisbet[1]

[1]Department of Earth Sciences, Royal Holloway, University of London, Egham, UK, [2]School of Geography, Earth and Environmental Sciences, University of Birmingham, Birmingham, UK, [3]Birmingham Institute of Forest Research, University of Birmingham, Birmingham, UK, [4]Centre for Oceanic and Atmospheric Sciences, School of Environmental Sciences, University of East Anglia, Norwich, UK, [5]Centre for Atmospheric Science, University of Cambridge, Cambridge, UK, [6]Department of Aerospace Engineering, University of Bristol, Bristol, UK, [7]School of Geographical Sciences, University of Bristol, Bristol, UK

Abstract Ascension Island is a remote South Atlantic equatorial site, ideal for monitoring tropical background CH_4. In September 2014 and July 2015, octocopters were used to collect air samples in Tedlar bags from different heights above and below the well-defined Trade Wind Inversion (TWI), sampling a maximum altitude of 2700 m above mean sea level. Sampling captured both remote air in the marine boundary layer below the TWI and also air masses above the TWI that had been lofted by convective systems in the African tropics. Air above the TWI was characterized by higher CH_4, but no distinct shift in $\delta^{13}C$ was observed compared to the air below. Back trajectories indicate that lofted CH_4 emissions from Southern Hemisphere Africa have bulk $\delta^{13}C_{CH4}$ signatures similar to background, suggesting mixed emissions from wetlands, agriculture, and biomass burning. The campaigns illustrate the usefulness of unmanned aerial system sampling and Ascension's value for atmospheric measurement in an understudied region.

1. Introduction

Global atmospheric methane (CH_4) is increasing rapidly. Between 2007 and 2013 CH_4 increased globally by 5.7 ± 1.7 ppb yr^{-1} with a more rapid increase in the equatorial tropics in 2010–2011. In 2014 the yearly growth increased to 12.5 ± 0.4 ppb [*Nisbet et al.*, 2016]. Tropical emissions are thought to be a major contributor to this growth [*Nisbet et al.*, 2014; *Schaefer et al.*, 2016]. Natural tropical sources include wetlands and other freshwater systems, lightning-lit fires, geological leaks, termites, and wild ruminants [*Dlugokencky et al.*, 2011]. CH_4 emissions from the tropics produce around ~200 Tg/yr which is thought to be about 40% of the global CH_4 budget [*Frankenberg et al.*, 2008; *Bousquet et al.*, 2006]. Variability in CH_4 removal through reaction with OH radicals is also dominated by the tropics as photochemistry is active throughout the year [*Bousquet et al.*, 2006].

$\delta^{13}C_{CH4}$ isotope ratios can be used to help apportion emission sources, because the different sources of CH_4 have different ratios of ^{13}C and ^{12}C isotopes. Background ambient air at present approximately has a $\delta^{13}C_{CH4}$ of -47.4 to -47.2‰ [*Nisbet et al.*, 2016]. CH_4 emissions from biological sources are depleted in comparison to background ambient air, for example, swamps give a signature of -55 ± 3‰ [*Dlugokencky et al.*, 2011], because methanogenic archaea preferentially use the lighter ^{12}C isotope. CH_4 formed at higher temperatures is relatively enriched in the heavier isotope, for example, biomass burning of savannah grassland (C4 plants) gives a signature of -20 to -15‰ [*Kirschke et al.*, 2013; *Dlugokencky et al.*, 2011; *Chanton et al.*, 2005]. See supporting information (S) Table S1 [*Teh et al.*, 2005; *Dlugokencky et al.*, 2011; *Chanton et al.*, 2000] for isotopic CH_4 source values for tropical wetlands and biomass burning.

In situ sampling of carbon isotopes in CH_4 can be used to distinguish sources [*Dlugokencky et al.*, 2011]. Apart from short airborne campaigns, such measurements have, however, usually been confined to within the planetary boundary layer. Unmanned aerial systems (UASs) offer a practical option for regular sampling at higher level. Aircraft measurements and flask sampling [*Schuck et al.*, 2012] are not practical for regular (daily or subdaily) sampling and are also limited by their rate of vertical and horizontal movement and hovering

abilities [*Chang et al*., 2016]. Balloon flights lack maneuvrability compared to UASs [*Karion et al*., 2010; *Chang et al*., 2016]. AirCore-like systems [*Karion et al*., 2010] are impractical for routine monitoring of $\delta^{13}C_{CH4}$ and mole fraction as it is difficult to achieve sufficient isotopic precision to observe small changes.

In this study, a new approach to sampling air masses at different heights using bespoke octocopters (UAS) was developed during two field campaigns on Ascension Island in September 2014 and July 2015. The target was to sample above the Trade Wind Inversion (TWI), a strong and persistent temperature inversion capping the marine boundary layer at altitudes between 1200 and 1800 m above sea level (asl) [*Barry and Chorley*, 2009]. There is strong wind shear across the TWI with air trajectories indicating different origins for air above and below the inversion, as discussed in section 1.1 below.

Air masses were sampled at various heights above and below the TWI, using a remotely controlled pump and valve system to fill Tedlar bags, probing air from different origins. Ascension Island's location is ideal for these experiments. The work has proved the ability of using UASs to collect and maintain the integrity of air samples using real time sensors for targeting specific air profile characteristics.

1.1. Ascension Island

Ascension Island (7°58'S, 14°24'W) (supporting information Text S1 and Figure S1), in the South Atlantic, experiences near constant South East Trade winds below the TWI (Figure S1a) [*Rolph*, 2016; *Stein et al*., 2015] with little diurnal variation, bringing air from central South America and the Southern Ocean. From Ascension the air crosses the Atlantic to become background into Amazonia. Above the TWI, air trajectories are quite different, and the air comes predominantly from tropical and southern Africa (Figure S1b). Ascension Island is therefore ideally located to measure the tropical Atlantic background air in the boundary layer and to study African sources of CH_4 by sampling the midtroposphere above the TWI.

Cumulative 240 h monthly backtrajectories were simulated for both the September and July campaign period using the NOAA Hybrid Single-Particle Lagrangian Integrated Trajectory (HYSPLIT) trajectory tool [*Stein et al*., 2015]. Air masses at ground level in September and July are from the remote South Atlantic, and above the TWI are from central and West Africa (Figures S1e–S1h) [*Rolph*, 2016; *Stein et al*., 2015].

Royal Holloway, University of London (RHUL), hosted by the UK Met Office, has measured CH_4 mole fractions (in situ) and $\delta^{13}C_{CH4}$ (in flasks) on Ascension Island from 2010 [*Nisbet et al*., 2016]. NOAA and the University of Colorado's Institute of Arctic and Alpine Research have measured both CH_4 mole fractions and $\delta^{13}C_{CH4}$ in flasks collected on the island since 2000 (Figure S2) [*Nisbet et al*., 2016; *Dlugokencky et al*., 2016; *White et al*., 2015].

2. Methods/Experimental Design

Three 8-rotor multirotor (octocopter) (Figure S3a) platforms were built from off the shelf components at the University of Bristol. The platforms were custom designed to carry gas sampling equipment and temperature and humidity response sensors to an altitude of 2700 m within 20 min, with 20% battery capacity remaining on landing. The meteorological sensors sent data to the ground control station in real time to allow targeted gas sampling during descent. Flight and avionic specifications of the platform [*Greatwood et al*., 2016] are detailed in Table S2 and key elements of the operational manual in Text S1 [*Thomas et al*., 2012].

Octocopters were flown from a site at 340 m asl (Figure S1c) with a maximum climb rate of 5 m/s. The system retrieved an in situ air sample using an on board diaphragm pump with a flow rate of 4.5 L/min to fill either 3 L or 5 L Tedlar bags (SKC Ltd) as the octocopter hovered for between 45 and 60 s, dependent on atmospheric pressure at the sampling altitude. It was possible to fill two samples per flight at different altitudes. A longer sampling time with a single bag was used at higher altitude ensuring enough sample mass was drawn into the bag for measurement.

High temporal resolution atmospheric profiles of temperature and humidity were telemetered to ground station computers during ascent. The TWI is characterized by temperature increase and relative humidity decrease above the cloud layer. This informed in-flight targeting decisions by the ground observer with remote communication to the UAS for the desired sampling altitude around the unexpectedly tightly defined TWI during the descent leg of the flight. Heights were accurate to within a few meters and allowed samples to be taken above, below, and within the TWI each day, avoiding the use of more uncertain model predictions of

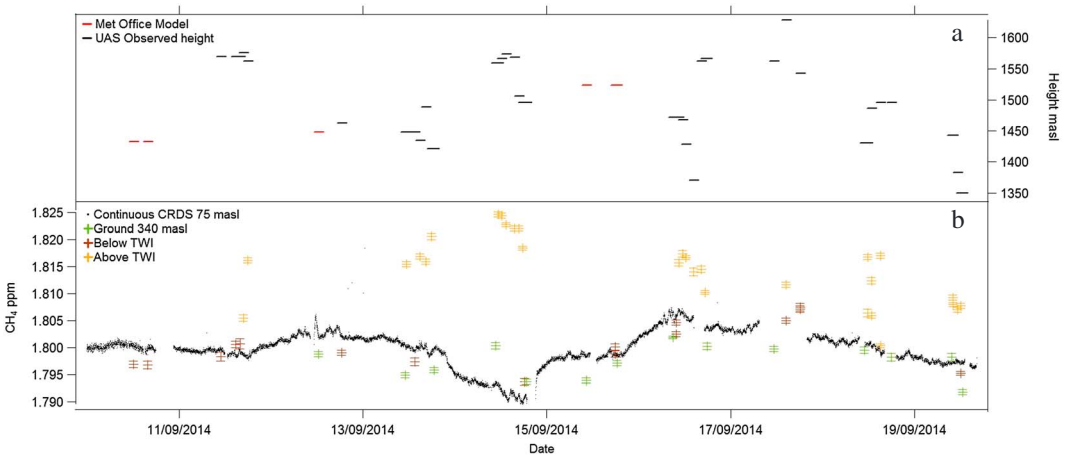

Figure 1. (a) The boundary layer heights per day calculated from either the temperature and humidity sensors on the UAS (black) or from the Met Office model (red). (b) Continuous CRDS CH_4 ground level (75 m asl) compared with bag samples taken during the September 2014 campaign, date markers denote 00 Coordinated Universal Time (UTC). The correlation between CRDS values and ground bag samples $r^2 = 0.558$ where critical $r^2 = 0.247$ at 0.05 significance. The bag samples have a negative bias of 2 ppb compared to the continuous CRDS values perhaps due to the sampling height difference. Using the difference between the median and the 95th percentile of the ground, below TWI, and above the TWI samples as a benchmark; ground level values give a difference of 3 ppb, below the TWI gives a difference of 7 ppb, and above the TWI mixing ratios gives a difference of 8 ppb. The difference of the median mixing ratios below and above the TWI is 16 ppb.

the TWI boundary (Figure S3b). Additional 3 L Tedlar bags were filled with air from approximately 1 m above site ground level (340 m asl) and Met Office ground level (75 m asl) each day to compliment the UAS samples. Samples from the flights and ground sampling were subsequently analyzed together, (see Text S2 [*Lowry et al*., 2014; *Fisher et al*., 2006; *Jones et al*., 2007; *Cullen*, 1993] for methods).

3. Results

NOAA and RHUL measurements show that the CH_4 mole fraction at Ascension has been increasing sharply since 2007 [*Nisbet et al*., 2016]. A parametric curve fitting program, HPspline, was used to assess the longer-term trends of the RHUL data using the parameters suggested in *Pickers and Manning* [2015]. Yearly deseasonalized trends show an increase in 2011–2012 of 4.36 ± 0.6 ppb, a slower increase of 3.91 ± 0.4 ppb in 2012–2013, a renewed larger increase of 6.68 ± 1.3 ppb in 2013–2014, and an increase of 12.67 ± 2.3 ppb in 2014–2015 (Figures S2 and S4) [*Nisbet et al*., 2016]. Continuous cavity ring-down spectroscopy (CRDS) monitoring of CH_4 shows regular dip and peak events (Figure S5). Peak events occur intermittently, with an increase of around 10 ppb and may last for a period of hours or days. A number of dip and peak events in CH_4 mole fraction occur even though the trajectories below the TWI are steady. The field campaigns were in September 2014 and July 2015. July was chosen as a comparison to the September campaign as July is normally the peak biomass burning season in Southern Hemisphere Africa [*Roberts et al*., 2009], when smoke plumes inject upward into the free troposphere [*Chatfield et al*., 1998].

3.1. Campaign 1—September 2014

The September 2014 campaign period overlaps with one of the numerous dip and peak events with a decline in the average mole fraction measured by the CRDS of 8 ppb on 14 September 2014 then a 6 ppb increase on 15 September 2014 of followed by a further 7 ppb increase on 16 September 2014 (Figures 1b and S9a). There are significant correlations (95% confidence) between the bag sample ground values collected at the UAS site, 340 m asl, and in situ measurements at 75 m asl showing no significant difference between the two sites.

Samples taken above the TWI have a higher CH_4 mole fraction than samples taken below (Figures 1b and 2). The samples retrieved from above the TWI contain higher CH_4 mixing ratios than ground level; however, during periods of lower mixing ratio of CH_4 at ground level there is an increased change in concentration across the TWI. The spread of CH_4 mixing ratios when compared over the whole campaign increases with altitude. No distinct isotope ratio change was seen between samples taken above or below the TWI. Ground values

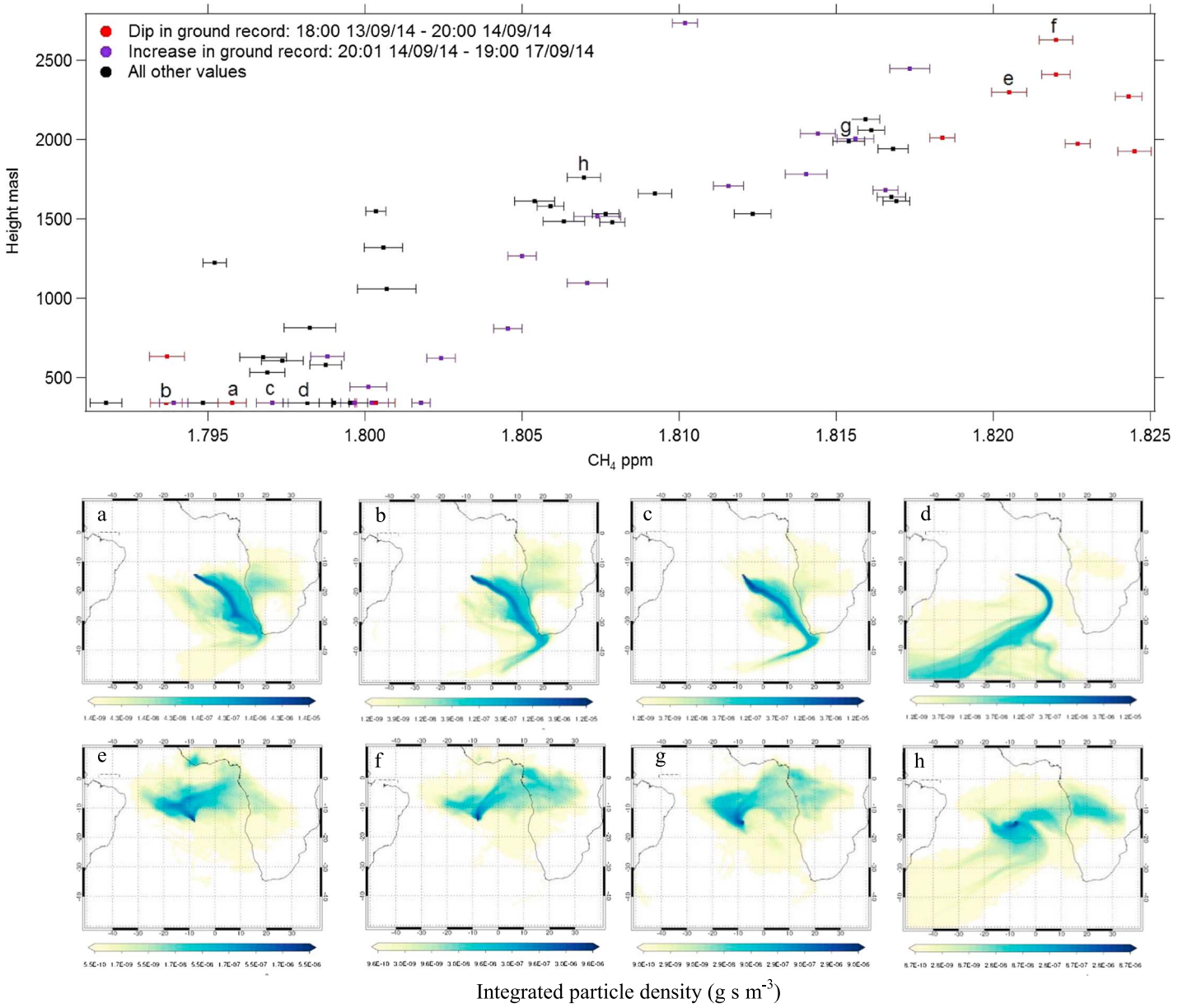

Figure 2. September 2014 bag samples plotted with height meters above sea level compared to typical NAME plots for each period. The NAME models are run for 7 days back from the sample collection time and height. Letters a–h on the graphs compare to the NAME plots. (a) The 13 September 2014 18:34 340 m asl, (b) 14 September 2014 18:40 340 m asl, (c) 15 September 2014 18:20 340 m asl, (d) 19 September 2014 09:45 340 m asl, (e) 13 September 2014 18:01 2298 m asl, (f) 14 September 2014 16:42 2629 m asl, (g) 16 September 2014 10:31 2008 m asl, and (h) 19 September 2014 11:07 1761 m asl.

ranged between −47.41 and −47.17‰ with samples taken from the UAS ranging between −47.60 and −47.00‰ (see Figure 5). Boundary layer heights (Figure 1) vary between 1350 and 1628 m asl with no correlation between boundary layer height and changes in the CH_4 mole fraction at ground level.

Daily NAME modeled footprint plots (Figure S6) have been generated from particles released from a height of 0 to 100 m above ground level with time integrated particle density in the boundary layer over the 11 days up to the release time. These plots show air arriving from the remote South Atlantic, and to a lesser extent from southern Africa as indicated in the cumulative trajectories.

NAME was run backward for 7 days for individual samples. Particles were released from the sample location (from a depth of 100 m centered on the sample height) in order to model where the measured air had come from. Figure S7 shows all the 7 day integrated particle density plots for each sample, for three different height

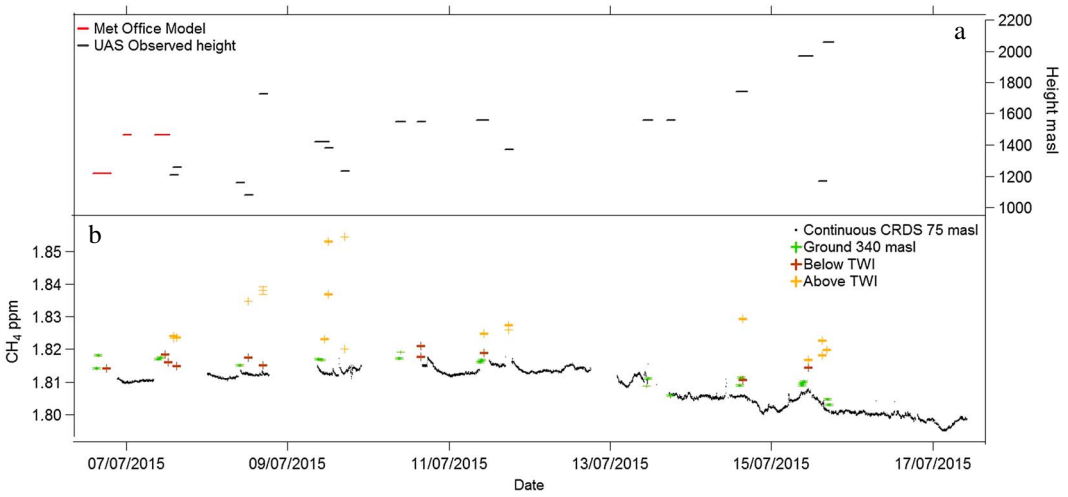

Figure 3. (a) The boundary layer heights calculated either from the temperature and humidity sensors on the UAS (black) or from the Met Office model (red). (b) Continuous CRDS CH_4 ground level (75 m asl) compared with bag samples taken during the July 2015 campaign. The correlation between CRDS values and ground bag samples $r^2 = 0.77$ where critical $r^2 = 0.171$ at a 0.05 significance. The bag samples have a negative bias of 1 ppb compared to the continuous CRDS values perhaps due to the sampling height difference. Using the difference between the median and the 95th percentile of the ground, below TWI, and above the TWI samples as a benchmark; ground level values give a difference of 4 ppb, below the TWI gives a difference of 5 ppb, and above the TWI mixing ratios gives a difference of 28 ppb. The difference of the median mixing ratios below and above the TWI is 8 ppb and the 95th percentile mixing ratios is 31 ppb.

bands (0.1–1 km, 1–3 km, and 3–9 km). Each plot shows the density of particles that passed through that grid box and height band over the last week. Clear differences can be seen in the air mass histories of different samples with variable influence from the different height layers. Some samples are mainly influenced by the remote South Atlantic, whereas others include air masses coming from the north or central Africa. Figure 2 shows typical NAME plots during each sampling period. Ground samples (Figures 2a to 2d) in general arrive from the remote South Atlantic. Above the TWI samples with influence from the east and northeast with air coming from over Africa (Figures 2e–2g and S7) tend to have higher mole fractions than those with South Atlantic influence (Figure 2h).

3.2. Campaign 2—July 2015

Continuous CRDS ground level measurements (Figure 3b) were on average 8 ppb higher in July 2015 than in September 2014. July 2015 ground samples have a larger range from 1800 to 1820 ppb before the drop of mole fraction on 13 July 2015 after which they range from 1795 to 1810 ppb, whereas the September 2014 campaign mole fractions were between 1790 and 1805 ppb (Figure S9). In contrast to the September campaign the samples taken above the TWI have a higher CH_4 mole fraction during the period when CH_4 is high at ground level (Figure 3). There is significant correlation between samples taken from the ground at both the UAS (340 m asl) and Met Office (75 m asl) sites and the Picarro CRDS values.

Boundary layer heights (Figure 3a) range from 1000 to 1500 m asl between 7 July 2015 and 11 July 2015. During the decrease in the ground level mole fraction beginning on 13 July 2015 the boundary layer height increases from ~1500 to ~2050 m asl.

Ground level mole fraction measurements can be separated into three periods in the July campaign (Figure 4ii); 6–12 July has the highest ground mole fractions and more enriched $\delta^{13}C_{CH4}$, 13–14 July is an intermediate period, and 15 July has lowest ground mole fraction and depleted $\delta^{13}C_{CH4}$ values (Figures 3b and 4). During the 6–12 July back trajectories on the ground show the air masses have a higher possibility of arrival from over Africa (Figures 4a and 4b) or from the remote South Atlantic (Figures 4 and S8).

4. Campaign Comparisons

Both campaigns show consistently higher CH_4 mole fractions above the TWI with increments up to 31 ppb. NAME modeling indicates these air masses may be influenced by source emissions north of the intertropical

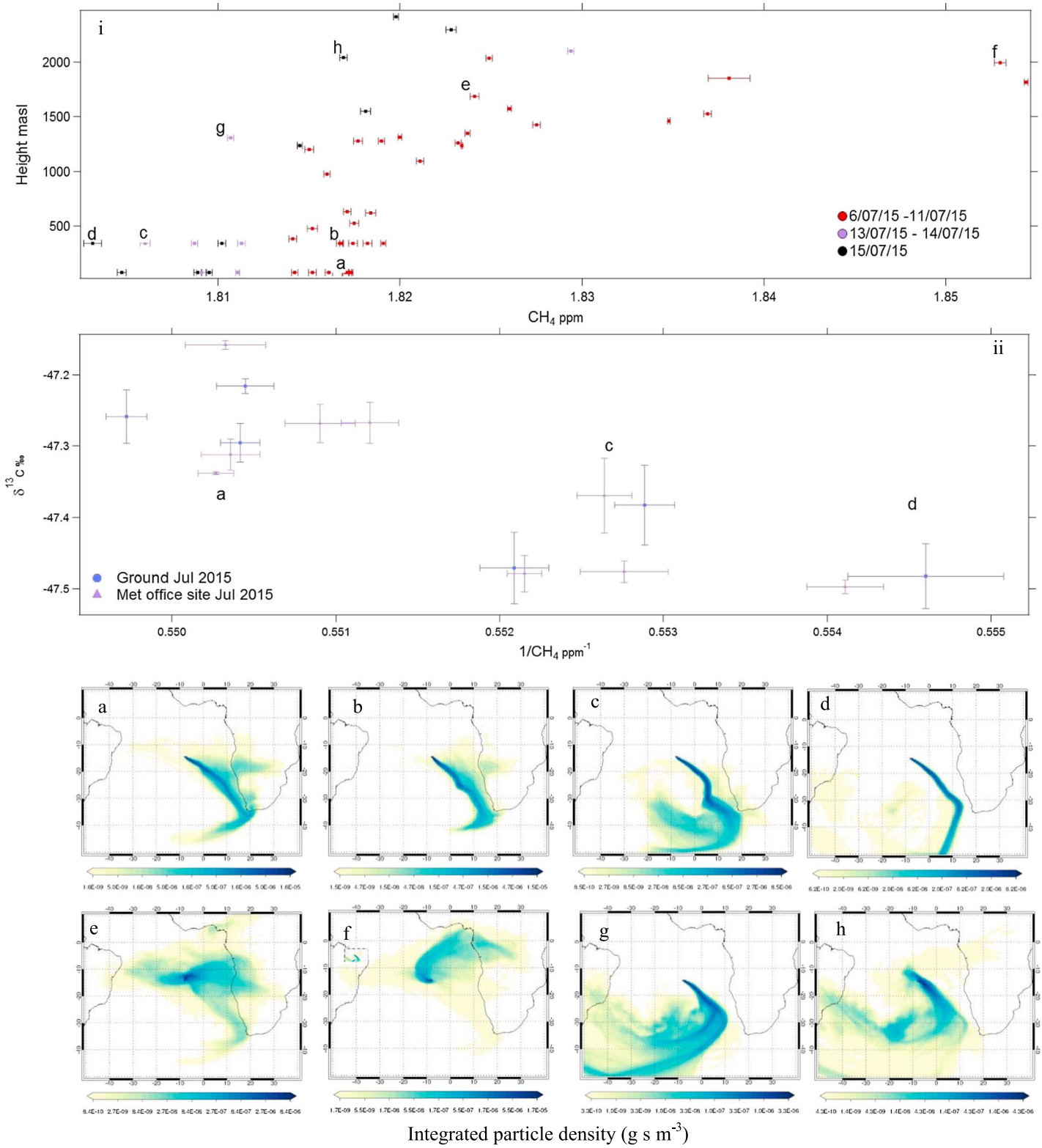

Figure 4. i: July 2015 bag samples plotted with height meters above sea level compared to typical NAME plots for each period. Letters a–h on the graphs compare to the NAME plots. The NAME models are run for 7 days back from the sample collection time and height: (a) 08 July 2015 09:38 75 m asl, (b) 09 July 2015 09:55 340 m asl, (c) 13 July 2015 17:50 340 m asl, (d) 15 July 2015 17:00 340 m asl, (e) 07 July 2015 14:00 1686 m asl, (f) 09 July 2015 12:00 1996 m asl, (g) 14 July 2015 15:30 1309 m asl, and (h) 15 July 2015 11:00 2044 m asl. ii. Plot showing the isotopic ground level values taken during July 2015. The $\delta^{13}C_{CH4}$ is plotted against the inverse of the concentration [*Pataki et al.*, 2003]. These periods are compared to the NAME plots.

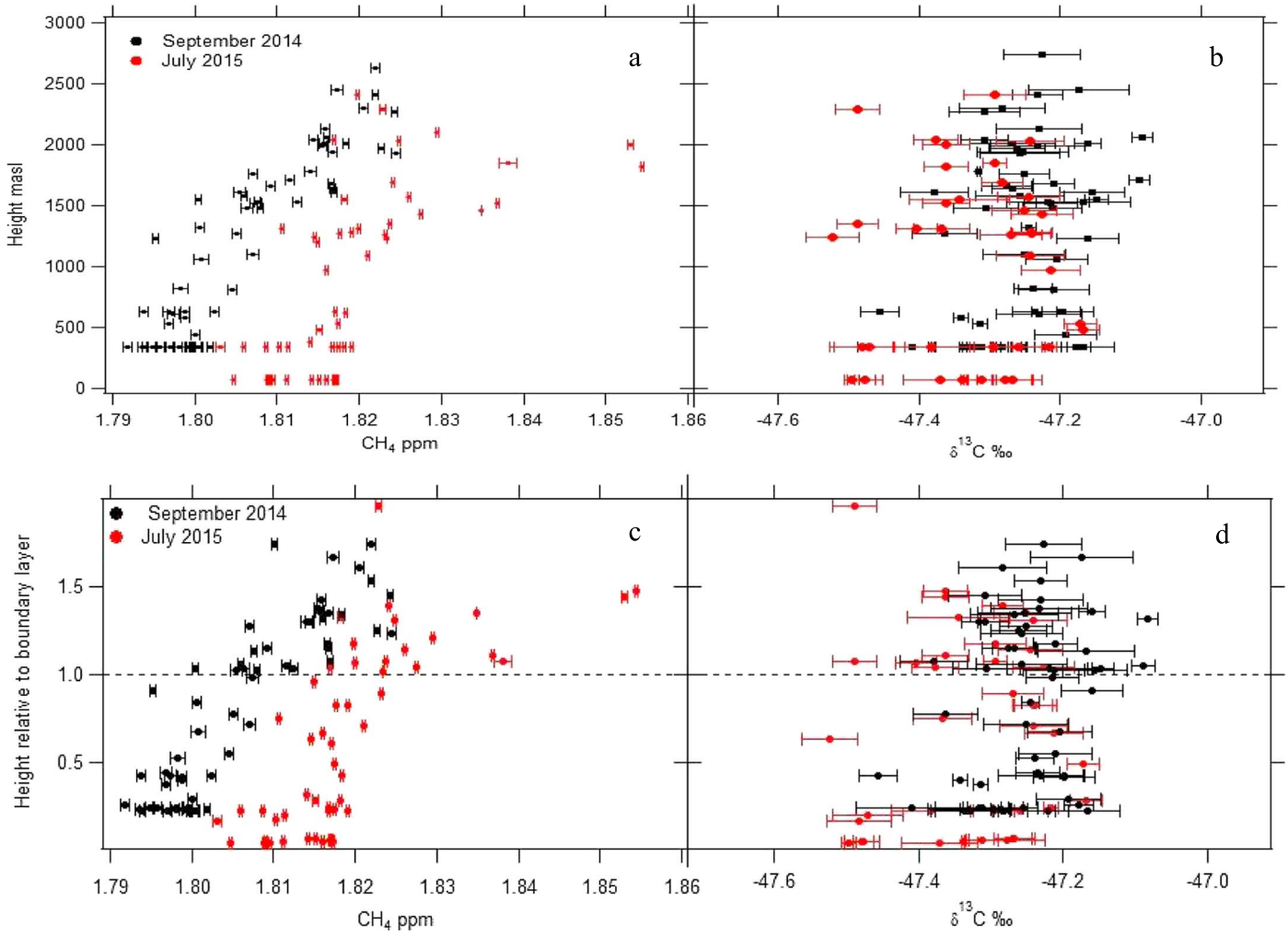

Figure 5. (a) Comparison of CH4 mole fraction variation with altitude for two field campaigns in September 2014 and July 2015. (b) Comparison of $\delta^{13}C_{CH4}$ variation with altitude between the two field campaigns in September 2014 and July 2015. Errors bars denote 1 standard deviation of the CRDS measurements for each sample (Text S2). (c) Comparison of CH_4 mole fraction with the sample height relative to the boundary layer. (d) Comparison of $\delta^{13}C_{CH4}$ variation with the sample height relative to the boundary layer. Each error bar denotes 1 standard deviation of triplicate measurements (Text S2).

convergence zone and air lofted above Africa by large-scale convection [e.g., *Schuck et al.*, 2012]. Samples from July 2015 have higher mole fractions and ranges compared to samples from September 2014 (Figure 5). This may reflect year-on-year growth and seasonality. There is expected to be more biomass burning ($\delta^{13}C$ heavy), as shown in the ground level samples (Figure 4ii) and wetland ($\delta^{13}C$ light) influence from southern Africa in July [*Roberts et al.*, 2009].

Different mixing rates across the TWI are suggested by the increase in mole fraction above the TWI during periods with lower ground values and a decrease in mole fraction above the TWI when higher ground values occurred in the September campaign. Trajectories above the TWI also show a NE component during the dip in ground level mole fraction compared to before and after the dip event. The three ground mole fraction periods shown in Figure 4ii during the July campaign shows that the mole fractions measured above the TWI were higher when higher ground values occurred suggesting the ground mole fraction was influenced by increments along the air mass trajectory.

During the July campaign there was a greater TWI height range (1030 to 2057 m asl). When the inversion is higher, the inversion strength is weaker with more mixing across the boundary layer [*Cao et al.*, 2007]. The 7–11 July campaign showed a larger CH_4 contrast above and below the TWI, indicating a stronger capping of the TWI with less mixing with the free troposphere. On the 15 July, the TWI height was higher, and there was less CH_4 mole fraction contrast across the TWI. The September campaign had more constant TWI height,

suggesting mixing above and below the TWI occurred before the air reached Ascension during the periods where there is a lower mole fraction separation above and below the TWI.

Isotopic data give an average of $\delta^{13}C$ $-47.25 \pm 0.09‰$ during the September campaign and an average of $-47.33 \pm 0.09‰$ during the July campaign (Figure 5) The shift to more depleted values in July corresponds to the long-term trend both on Ascension Island and globally. Overall, no distinct isotopic ratio change was seen above the TWI during either of the campaigns (Figures 5 and S10) [*Pataki et al*., 2003]. Figures 5i, 5f, and 5h show two samples at a similar height above the TWI with air masses arriving from different source regions. Sample f has a trajectory with a higher possibility of inputs from African emissions and has a CH_4 mole fraction of 1853 ppb and $\delta^{13}C$ $-47.36‰$. Sample h has a trajectory predominately from over the South Atlantic and a CH_4 mole fraction of 1817 ppb and $\delta^{13}C$ $-47.38‰$. There is an input of 36.1 ppb CH_4 from African sources but an isotopic shift of only 0.02‰ suggesting the sources (Table S1) have a combined isotopic signature close to the bulk atmospheric value. A mixture of tropical wetland emissions ($-55 \pm 3‰$), agriculture ($-62 \pm 3‰$), and biomass burning of savannah grassland (-20 to $-15‰$) [*Dlugokencky et al*., 2011] would fit. Destruction by OH is the main CH_4 sink; this has a kinetic isotope shift of 4 to 6‰ [*Allan et al*., 2001, 2007; *Nisbet et al*., 2016]. However, the lifetime of CH_4 is ~9 years [*Dlugokencky et al*., 2011] so even in the intense OH of the tropical mid-troposphere the effect of OH destruction between the African sources and Ascension Island is small. A more local influence may be from the marine Cl sink in the marine boundary layer [*Allan et al*., 2001, 2007].

5. Conclusions

Ground values, taken more frequently during the campaigns, show a wider spread of isotopic signatures than the long-term bimonthly RHUL samples [*Nisbet et al*., 2016], making it more difficult to identify a distinct isotopic change above the TWI. The September ground values have a range of 10 ppb and 0.33‰, and the July ground values have a range of 17 ppb and 0.24‰. This may suggest an influence from possible local factors such as the little studied Cl sink or varied OH loss. Sink processes preferentially remove $^{12}C_{CH4}$ [*Schaefer et al*., 2016]. The air mass footprints have varying influences from Africa as well as the remote South Atlantic likely contributing to the isotopic changes.

NAME modeling has shown that the air mass origin above the TWI can vary daily. Both the origin of air masses and mixing events above and below the TWI influence the mole fractions of the ground samples. The isotopes have no consistent signal above or below the TWI, despite the significant CH_4 increment measured indicating the input from Africa is close to background $\delta^{13}C$. This input is likely to be a mixture of emissions from tropical wetlands, agriculture, and biomass burning. The samples taken higher up may be more influenced by these diverse sources over Africa.

Longer-term regular monitoring above the TWI would be useful for identifying isotopic signatures of the mixed tropical sources from Africa, determining seasonality and long-term trends. During such monitoring, replacing Tedlar bags with aluminum flask samples would allow CO/CO_2 to be monitored, which perhaps along with absorbing aerosol measurements would help characterize air masses according to biomass burning history. Other measurements such as water vapor mixing ratios and $^{18}O/^{16}O$ [*Bailey et al*., 2013], or O_3/CO_2 ratios [*Berkes et al*., 2016], could allow quantification of vertical mixing over the TWI and aid interpretation of CH_4 isotopic composition. If a UAS were to be used, an increase of approximately 30% in the mass should allow these changes to be realized.

Relatively lightweight sensors (1–2 kg) may be placed on a UAS to measure the CH_4 concentration although the precision of ~1% is not sufficient to detect small changes in ambient air [*Kahn et al*., 2012]. A precision of at least 5 ppb would be needed to distinguish differences across the TWI and a higher precision for smaller mole fraction changes associated with meteorological factors. It is likely that such instrumentation will be developed in the next few years.

Overall, the campaigns have shown that it is possible to use inexpensive UASs to access the midtroposphere above Ascension Island and retrieve air samples. Sampling at Ascension is able to measure both remote South Atlantic air from below the trade wind inversion and also air from above that has been lofted by convective systems in a wide region of the equatorial and southern savannah tropics. Thus, the technique extends Ascension's access from sea level up to 2700 m asl, making it a superb location for long-term global monitoring.

Acknowledgments

This work was part of the investigation of the southern methane anomaly: causes, implications, and relevance to past global events funded by the UK Natural Environment Research Council (NERC) (grant NE/K006045/1) and NERC studentship. Thanks to support from the Met Office, RAF, and USAF on Ascension Island. The authors gratefully acknowledge the NOAA Air Resources Laboratory (ARL) for the provision of the HYSPLIT transport and dispersion model and/or READY website (http://www.ready.noaa.gov) used in this publication. Data will be deposited in the UK Centre for Environmental Data Analysis on completion of Rebecca Brownlow's PhD thesis. We acknowledge use of the NAME atmospheric dispersion model and associated NWP meteorological data sets made available to us by the Met Office. We acknowledge the significant storage resources and analysis facilities made available to us on JASMIN by STFC CEDA along with the corresponding support teams.

References

Allan, W., H. Struthers, and D. C. Lowe (2007), Methane carbon isotope effects caused by atomic chlorine in the marine boundary layer: Global model results compared with Southern Hemisphere measurements, *J. Geophys. Res.*, *112*, D04306, doi:10.1029/2006JD007369.

Allan, W., M. R. Manning, K. R. Lassey, D. C. Lowe, and A. J. Gomez (2001), Modeling the variation of $\delta^{13}C$ in atmospheric methane: Phase ellipses and the kinetic isotope effect, *Global Biogeochem. Cycles*, *15*(2), 467–481, doi:10.1029/2000GB001282.

Bailey, A., D. Toohey, and D. Noone (2013), Characterizing moisture exchange between the Hawaiian convective boundary layer and free troposphere using stable isotopes in water, *J. Geophys. Res. Atmos.*, *118*, 8208–8221, doi:10.1002/jgrd.50639.

Barry, R. G., and R. J. Chorley (2009), *Atmosphere, Weather and Climate*, Routledge, New York.

Bousquet, P., et al. (2006), Contribution of anthropogenic and natural sources to atmospheric methane variability, *Nature*, *443*(7110), 439–43, doi:10.1038/nature05132.

Berkes, F., P. Hoor, H. Bozem, D. Kunkel, M. Sprenger, and S. Henne (2016), Airborne observation of mixing across the entrainment zone during PARADE 2011, *Atmos. Chem. Phys.*, *16*, 6011–6025.

Cao, G., T. W. Giambelluca, D. E. Stevens, and T. a. Schroeder (2007), Inversion variability in the Hawaiian trade wind regime, *J. Clim.*, *20*(7), 1145–1160, doi:10.1175/JCLI4033.1.

Chang, C. C., J. L. Wang, C. Y. Chang, M. C. Liang, and M. R. Lin (2016), Development of a multicopter-carried whole air sampling apparatus and its applications in environmental studies, *Chemosphere*, *144*, 484–492, doi:10.1016/j.chemosphere.2015.08.028.

Chanton, J., L. Chaser, P. Glasser, and D. Siegel (2005), Carbon and hydrogen isotopic effects in microbial methane from terrestrial environments, in *Stable Isotopes and Biosphere Atmosphere Interactions*, edited by L. B. Flanagan, J. R. Ehleringer, and D. E. Pataki, Elsevier, Oxford.

Chanton, J. P., C. M. Rutkowski, C. C. Schwartz, D. E. Ward, and L. Boring (2000), Factors influencing the stable carbon isotopic signature of methane from combustion and biomass burning, *J. Geophys. Res.*, *105*, 1867, doi:10.1029/1999JD900909.

Chatfield, R. B., J. A. Vastano, L. Li, G. W. Sachse, and V. S. Connors (1998), The Great African Plume from biomass burning: Generalizations from a three-dimensional study of TRACE A carbon monoxide, *J. Geophys. Res.*, *103*, 28,059–28,077, doi:10.1029/97JD03363.

Cullen, M. J. P. (1993), The unified forecast climate model, *Meteorol Mag*, *122*(1449), 81–94.

Dlugokencky, E. J., P. M. Lang, A. M. Crotwell, J. W. Mund, M. J. Crotwell, and K. W. Thoning (2016). Atmospheric methane dry air mole fractions from the NOAA ESRL carbon cycle cooperative global air sampling network, 1983–2015, Version: 2016-07-07. [Available at ftp://aftp.cmdl.noaa.gov/data/trace_gases/ch4/flask/surface/.]

Dlugokencky, E. J., E. G. Nisbet, R. Fisher, and D. Lowry (2011), Global atmospheric methane: Budget, changes and dangers, *Phil. Trans. R. Soc. A*, *369*(1943), 2058–72, doi:10.1098/rsta.2010.0341.

Fisher, R. E., D. Lowry, O. Wilkin, S. Sriskantharajah, and E. G. Nisbet (2006), High precision, automated stable isotope analysis of atmospheric methane and carbon dioxide using continuous-flow isotope-ratio mass spectrometry, *Rapid Commun. Mass Spectrom.*, *20*(2), 200–8, doi:10.1002/rcm.2300.

Frankenberg, C., P. Bergamaschi, A. Butz, S. Houweling, J. F. Meirink, J. Notholt, A. K. Petersen, H. Schrijver, T. Warneke, and I. Aben (2008), Tropical methane emissions: A revised view from SCIAMACHY onboard ENVISAT, *Geophys. Res. Lett.*, *35*, L15811, doi:10.1029/2008GL034300.

Greatwood, C., Richardson, T., J. Freer, R. Thomas, R. Brownlow, D. Lowry, R. E. Fisher, and E. G. Nisbet (2016). Automatic path generation for multirotor descents through varying air masses above Ascension Island. *AIAA Atmospheric Flight Mechanics Conference*, (January 2016), 1–12, doi:10.2514/6.2016-1532.

Jones, A. R., D. J. Thomson, M. Hort, and B. Devenish (2007), The U.K. Met Office's next-generation atmospheric dispersion model, NAME III, in *Air Pollution Modeling and Its Application XVII* (Proceedings of the 27th NATO/CCMS International Technical Meeting on Air Pollution Modelling and its Application), edited by C. Borrego and A.-L. Norman, pp. 580–589, Springer.

Kahn, A., D. Schaefer, L. Tao, D. J. Miller, K. Sun, M. A. Zondlo, W. A. Harrison, B. Roscoe, and D. J. Lary (2012), Low power greenhouse gas sensors for unmanned aerial vehicles, *Remote Sens.*, *4*(5), 1355–1368, doi:10.3390/rs4051355.

Karion, A., C. Sweeney, P. Tans, and T. Newberger (2010), AirCore: An innovative atmospheric sampling system, *J. Atmos. Oceanic Technol.*, *27*(11), 1839–1853, doi:10.1175/2010JTECHA1448.1.

Kirschke, S., P. Bousquet, P. Ciais, M. Saunois, J. G. Canadell, E. J. Dlugokencky, and G. Zeng (2013), Three decades of global methane sources and sinks, *Nat. Geosci.*, *6*(10), 813–823, doi:10.1038/ngeo1955.

Lowry, D., R.E. Fisher, J.L. France, M. Lanoisellé, E.G. Nisbet, E. Brunke, E. Dlugokencky, N. Brough and A. Jones (2014), Continuous monitoring of greenhouse gases in the South Atlantic And Southern Ocean: Contributions from the equianos network. 17th WMO/IAEA Meeting of Experts on Carbon Dioxide, Other Greenhouse Gases and related Tracers Measurement Techniques, GAW Report 213, Geneva, 109–112.

Nisbet, E. G., et al. (2016), Rising atmospheric methane: 2007–14 growth and isotopic shift, *Global Biogeochem. Cycles*, *30*, 1356–1370, doi:10.1002/2016GB005406.

Nisbet, E. G., E. J. Dlugokencky, and P. Bousquet (2014), Atmospheric science. Methane on the rise-again, *Science*, *343*(6170), 493–5, doi:10.1126/science.1247828.

Pataki, D. E., J. R. Ehleringer, L. B. Flanagan, D. Yakir, D. R. Bowling, C. J. Still, N. Buchmann, J. O. Kaplan, and J. A. Berry, (2003), The application and interpretation of Keeling plots in terrestrial carbon cycle research, *Global Biogeochem. Cycles*, *17*(1), 1022, doi: 10.1029/2001GB001850.

Pickers, P. A., and A. C. Manning (2015), Investigating bias in the application of curve fitting programs to atmospheric time series, *Atmos. Meas. Tech.*, *8*(3), 1469–1489, doi:10.5194/amt-8-1469-2015.

Roberts, G., M. J. Wooster, and E. Lagoudakis (2009), Annual and diurnal African biomass burning temporal dynamics, *Biogeosciences*, *6*, 849–866, doi:10.5194/bg-6-849-2009.

Rolph, G. D. (2016), Real-time Environmental Applications and Display sYstem (READY), NOAA Air Resources Laboratory, College Park, Md. [Available at http://www.ready.noaa.gov.]

Schaefer, H., et al. (2016), A 21st century shift from fossil-fuel to biogenic methane emissions indicated by $^{13}CH_4$, *Science*, *351*(6278), doi:10.1126/science.aad2705.

Schuck, T. J., K. Ishijima, P. K. Patra, A. K. Baker, T. Machida, H. Matsueda, Y. Sawa, T. Umezawa, C. A. M. Brenninkmeijer, and J. Lelieveld (2012), Distribution of methane in the tropical upper troposphere measured by CARIBIC and CONTRAIL aircraft, *J. Geophys. Res.*, *117*, D19304, doi:10.1029/2012JD018199.

Stein, A. F., R. R. Draxler, G. D. Rolph, B. J. B. Stunder, M. D. Cohen, and F. Ngan (2015), NOAA's HYSPLIT atmospheric transport and dispersion modeling system, *Bull. Am. Meteorol. Soc.*, *96*, 2059–2077, doi:10.1175/BAMS-D-14-00110.1.

Teh, Y. A., W. L. Silver, and M. E. Conrad (2005), Oxygen effects on methane production and oxidation in humid tropical forest soils, *Glob. Change Biol.*, *11*(8), 1283–1297, doi:10.1111/j.1365-2486.2005.00983.x.

Thomas, R. M., K. Lehmann, H. Nguyen, D. L. Jackson, D. Wolfe, and V. Ramanathan (2012), Measurement of turbulent water vapor fluxes using a lightweight unmanned aerial vehicle system, *Atmos. Meas. Tech.*, *5*, 243–257.

White, J. W. C., B. H. Vaughn, and S. E. Michel (2015), University of Colorado, Institute of Arctic and Alpine Research (INSTAAR), Stable Isotopic Composition of Atmospheric Methane (^{13}C) from the NOAA ESRL Carbon Cycle Cooperative Global Air Sampling Network, 1998–2014, Version: 2016-04-26. [Available at ftp://aftp.cmdl.noaa.gov/data/trace_gases/ch4c13/flask/.]